Article

Design Principles for Metastable Standing Molecules

Hadi H. Arefi, Daniel Corken, F. Stefan Tautz, Reinhard J. Maurer, and Christian Wagner*

Read Online

ACCESS |
📊 Metrics & More |
📖 Article Recommendations

ABSTRACT: Molecular nanofabrication with a scanning probe microscope (SPM) is a promising route toward the prototyping of metastable functional molecular structures and devices which do not form spontaneously. The aspect of mechanical stability is crucial for such structures, especially if they extend into the third dimension vertical to the surface. A prominent example is freestanding molecules fabricated on a metal which can function as field emitters or electric field sensors. Improving the stability of such molecular configurations is an optimization task involving many degrees of freedom and therefore best tackled by computational nanostructure design. Here, we use density functional theory to study 3,4,9,10-perylene-tetracarboxylic dia-nhydride (PTCDA) standing on the Ag(111) surface as well as on

the tip of a scanning probe microscope. We cast our results into a simple set of design principles for such metastable structures, the validity of which we subsequently demonstrate in two computational case studies. Our work proves the capabilities of computational nanostructure design in the field of metastable molecular structures and offers the intuition needed to fabricate new devices without tedious trial and error.
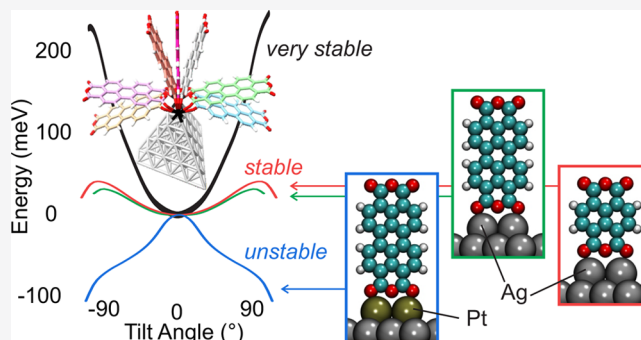
■ INTRODUCTION

The scanning probe microscope (SPM) is a powerful tool for nanofabrication, offering a promising long-term perspective for the prototyping of nanometer-scale functional molecular structures well beyond those accessible by self-assembly.[1−14] Metastable molecular configurations created by SPM-based manipulation can possess unique electronic and mechanical properties, making them interesting for new types of devices. Tip-attached standing molecules in scanning quantum dot microscopy (SQDM)[9,15] are, for example, one of the few actually useful single-molecule devices. Such examples show that a weak coupling between a molecule and its support can, in fact, be a necessary prerequisite for functionality[9,11,15,16] and thus an integral aspect of future molecular devices. When accepting this fact, stability becomes a crucial design issue because weak coupling often implies metastability. Typically, metastable molecular structures have to be fabricated and investigated at cryogenic temperatures of 5 K to suppress instability from thermal fluctuations.[17] If they could, however, reliably withstand higher temperatures, strong electric fields and other effects such as charging, the application range of molecular devices would greatly increase. Here, we demon-strate how computational nanostructure design using density functional theory (DFT) calculations allows us to discover and systematically improve suitable metastable molecular devices.

DFT is the workhorse of contemporary atomistic quantum mechanical calculations and an important complement to

experimental observations. Notably, it has provided insights into many metal−organic hybrid systems like molecular monolayers adsorbed on high-symmetry surfaces.[18−26] The capability of DFT to describe such systems has steadily improved, particularly due to a more sophisticated treatment of long-range van der Waals (vdW) interactions.[24,27−31] How-ever, the metastable conformations encountered in SPM-based nanofabrication (Figure 1) are substantially different from the monolayer systems that DFT is typically benchmarked against.

In a previous paper, we could, nevertheless, prove experimentally that the Perdew−Burke−Ernzerhof (PBE) functional[32] in combination with the many-body dispersion approach (MBD)[28−30] can accurately reproduce the potential energy landscape of a standing molecule.[17] Specifically, the computed barrier height of approximately 30 meV which prevents the collapse of a standing 3,4,9,10-perylene-tetracarboxylic dianhydride (PTCDA) molecule on adatoms on Ag(111) was confirmed by thermal excitation measure-ments. Since barrier heights are practically energy differences and not absolute energies, the accuracy of the respective
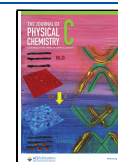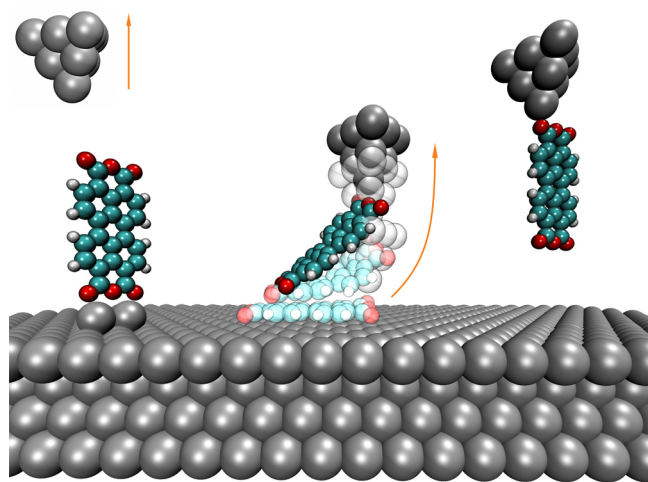
Figure 1. Fabrication of standing PTCDA. To bring PTCDA into a vertical conformation on the SPM tip (right) or the adatom surface (left), first a bond between the SPM tip and a O_{carb} atom of the surface-adsorbed molecule needs to be established. Upon tip retraction (center), either the molecule−surface connection breaks (right), or if a pedestal of two adatoms has been fabricated at the lower end of the molecule, the tip−molecule bond eventually breaks and the molecule remains vertically on the surface (left).

calculation is well below typical uncertainties of absolute DFT energies of ∼100 meV. While the 1−2 meV difference between theory and experiment in ref [17] is probably a fortuitous agreement, also larger discrepancies would have no negative effect on the conclusions and design rules derived here. This confirmation of our DFT method for one specific metastable configuration is a crucial prerequisite for the present in-depth study.

The standing PTCDA on Ag(111) is characterized by a competition between stabilizing covalent and destabilizing vdW interactions that causes a shallow potential energy minimum and thermally induced collapse between 10 and 14 K.[17] This insight is our starting point for a deeper and more detailed study culminating in the development of practically applicable design rules. To identify global trends, we examine a broad set of possible configurations of standing PTCDA (s-PTCDA), including cases in which PTCDA is attached to the SPM tip as is required for SQDM.[9,15,16] Due to the variable and experimentally inaccessible atomic structure of the SPM tip, it is not possible to determine the configuration of the PTCDA-tip bonding region unambiguously. By computationally exploring the potential energy surface of s-PTCDA on various tip apex structures, we can nevertheless reveal fundamental aspects of the PTCDA-tip attachment, like the number of involved Ag−O bonds.

Because the potential energy surface of *s*-PTCDA is the consequence of a competition between covalent and vdW interactions,[17] the design criteria for enhanced stability can be formulated with regard to these two interaction types. We have organized the paper accordingly: After summarizing the computational methods, discussing the experimentally observed properties of s-PTCDA and defining the set of SPM tip structures used in our analysis, we first analyze the chemical bonding of s-PTCDA to the Ag structures and subsequently the influence of the vdW interactions on stability. The deduced design criteria are finally validated in two computational case studies.

■ COMPUTATIONAL METHODS

DFT Calculations. We performed DFT calculations using the Fritz-Haber-Institute ab initio molecular simulation package (FHI-aims).[33] We used the semilocal exchange-correlation functional of Perdew, Burke, and Ernzerhof (GGA-PBE)[32] to treat the electronic exchange and correlation. To account for long-range dispersion interactions, we used the vdW^{surf} scheme[24,27,31] and the MBD method.[28−30] We use vdW^{surf} when exploring tip structures and MBD for our computational case studies where highly accurate vdW energies are beneficial. To include relativistic effects, we applied the scaled zeroth-order regular approximation (ZORA)[34] in all calculations.

Depending on whether the target system is an isolated cluster tip or a periodic slab, we treated them with either aperiodic or periodic boundary conditions, respectively. For the periodic slab calculations, we used a Γ-centered 2 × 2 × 1 Monkhorst−Pack grid[35] to sample the Brillouin zone during structural relaxation. It was replaced with a denser 4 × 4 × 1 mesh for PBE + vdW^{surf} or PBE + MBD production calculations and charge density difference analysis. For the MBD postprocessing calculations, the Brillouin zone was sampled with a half-Γ-shifted 8 × 8 × 1 K-point grid. To aid the convergence, we applied a 0.02 eV broadening to all states, using a Gaussian occupation smearing scheme.[36]

Using the Broyden−Fletcher−Goldfarb−Shanno (BFGS) algorithm, we relaxed the structures via two serial steps, first by expanding the Kohn−Sham wave function with the default numerical "light" basis sets,[37] applied to all atomic species. Once finished, all basis sets were replaced with the default numerical "tight" settings,[37] and the relaxation was resumed. We continued the relaxation until the maximum force on each atom, in either setup, was less than 10^{-3} eV/Å. To obtain a well-converged electronic description of the systems, a threshold of 10^{-7} eV for the total energy, 10^{-4} eV for the sum of eigenvalues, and 10^{-6} e/Å³ for the charge density was applied during all SCF cycles.

Tip Model Preparation. To prepare our tip models, we first built a ten-layer-thick 10 × 10 Ag(111) slab with the experimental lattice constant and the surface normal pointing along the z-axis. Subsequently, cluster tips were carved out of the slab by removing silver atoms until the desired shapes were achieved. For the two-atom apex tips, silver adatoms were considered with either the minimum lateral distance in *xy*, i.e., 2.88 Å (D_1) or slightly larger at 3.32 Å (D_2). Depending on the atom removal strategy applied to the upper layers, the created clusters resembled either rather sharp or blunt tips. Sharp tips are made by keeping always only the nearest-neighbor (NN) atoms with respect to the previous layer. To create blunt tips, we kept more than just NN atoms in the first layer beneath the apex, depending on how blunt and in what shape the tip model was supposed to be. From the second layer onward, we used the original protocol of keeping just the NN atoms. The single apex *Tip 1* is created with six atomic layers (including apex), while all other tips have five layers. Except for the apex atom and the layer above it, all silver atoms in the tip models are frozen during geometry relaxations.

Slab Preparation. To model the Ag(111) surface, we built a four-layer 8 × 8 silver slab consisting of 256 Ag atoms and a 60 Å thick vacuum layer added between slab images along the z direction. Starting from the experimental surface lattice constant (a = b = 2.88 Å), the lattice parameter was first
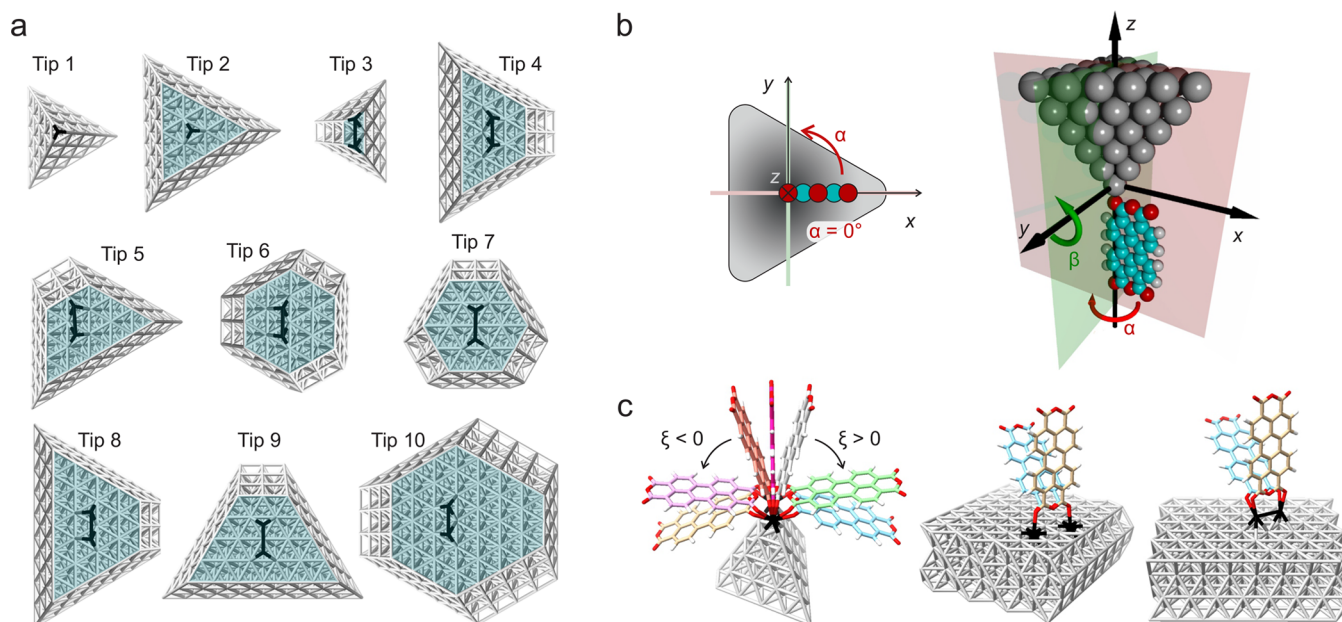
Figure 2. Tip models. (a) All tip models used in this study. The tip apex atoms which bind to PTCDA are colored black for visual enhancement. The flat area of each tip onto which the apex atoms are placed is highlighted. *Tip 1* and *Tip 2* feature a single apex atom, and all other tip models feature two apex atoms. (b) The geometries of PTCDA attached to a single-apex tip are defined by the angles α and β. Shown is the case of $\alpha = \beta = 0$ in a space-filling model of *Tip 1* (right) and in a schematic view along the positive z axis (left). (c) In the two-bond scenario, the geometries of PTCDA are defined by the angle ξ. Shown are exemplary geometries for PTCDA on *Tip 3* (left), bare Ag(111) (center), and the adatom surface (right). The tip models 3–10 in panel (a) are oriented such that positive ξ values always correspond to a tilting of the molecule to the right.

converged for a four-layer Ag(111) primitive unit cell, and the supercell was constructed accordingly. The converged lattice parameter ($a = b = 2.875$ Å) was very close to the experimental value. The adatom pedestal in the D_1 configuration was created by placing two Ag adatoms at neighboring hcp hollow sites 2.36 Å above the surface. Similar to the two-atom apex tips, we defined the reaction coordinate ξ for the rotation around the axis of adatoms as the angle between the plane of PTCDA and the surface normal. The bottom three layers of the slab were held fixed, while the top layer and the adatoms were allowed to relax freely.

One-Bond Scenario Configuration Mapping. In the one-bond scenario, the (azimuthal) angle α is measured between the short axis of PTCDA and the x axis, and the angle β is measured between the long axis of PTCDA and the z axis (Figure 2b). We map the potential energy surface for both tip models on a grid of 3 α values (0°, 90°, and 180°) and 21 β values in the interval $\beta = [-90°...90°]$, with ($\alpha = \beta = 0°$) denoting the strictly vertical alignment of PTCDA shown in Figure 2b. Configurations for which no stable constrained relaxation was possible, e.g., due to molecule–metal overlap, were, however, not considered further.

Constrained Optimization. For a proper mapping of the potential energy surface, structural relaxation is required while keeping the angles α and β of the molecule fixed. In the two-bond scenario, only ξ needs to be considered, and the constraint was imposed by fixing the z coordinate of a single carbon atom at the side of the PTCDA molecule far from the Ag–O_{carb} bond. Since the relaxation of the Ag–O_{carb} bond leads to a small change in ξ under this constraint, the value of ξ was remeasured once the structure was optimized, and the measured value was used in all plots. In the one-bond scenario, fixing α and β angles was achieved by constraining one coordinate of each of three carbon atoms of the perylene core

at the side of the PTCDA molecule opposite of the Ag–O bond. Again, after optimization, the tilt angle β was remeasured.

RESULTS AND DISCUSSION

Fabrication and Properties of Standing PTCDA. The design principles formulated in this theoretical study are validated by their capability to predict and explain experimentally observed properties of s-PTCDA. Particularly, the different behavior of s-PTCDA either on the Ag(111) surface or on the Ag-covered SPM tip (Figure 1) is of relevance in this respect. Here, we briefly describe the SPM-based fabrication process of each configuration and their experimentally observed properties.

Standing PTCDA on Ag(111) can be created by two-contact manipulation with the SPM tip,[11] where one contact is between the molecule and the tip and the second contact between the molecule and the surface. First, two Ag adatoms which later form a "pedestal" are attached to the two carboxylic oxygen atoms (O_{carb}) at the short side of PTCDA by lateral manipulation. Subsequently, PTCDA is contacted by the tip at one of the other two O_{carb} atoms and lifted into a vertical orientation. Further tip retraction breaks the tip–PTCDA bond, finalizing the assembly process (Figure 1, left). If, on the other hand, no Ag adatom pedestal is used and lifting of an isolated PTCDA molecule is performed (Figure 1, center), the molecule is detached from the surface and typically remains on the SPM tip in a likewise vertical orientation (Figure 1, right),[15,16,38−40] the detailed atomic configuration of which is experimentally inaccessible.

With this fabrication process, s-PTCDA is a prototypical SPM-fabricated metastable molecular configuration with properties that make it also a single-molecule device: On the Ag(111) surface, it functions as a single electron field emitter[11]

and GHz oscillator.[17] Tip-attached s-PTCDA, on the other hand, enables a new microscopy technique, SQDM.[9,15] All these functionalities are enabled by the metastable vertical configuration of s-PTCDA, which is characterized by a minimal overlap between the molecular π-system and tip or sample. Due to this minimal overlap, certain electronic states of the molecule remain decoupled from the metal and can be gated by applying a voltage to the tip–molecule–surface junction. At sufficiently high gate voltage, s-PTCDA can then acquire an additional positive or negative elementary charge[9,11,15,16] which is the fundamental mechanism enabling both SQDM and field emission from s-PTCDA. The weak mechanical coupling between s-PTCDA and the metal, on the other hand, allows the oscillation of the entire molecule with a remarkably low GHz frequency.[17]

The stability-related phenomenology of s-PTCDA on the tip and the surface becomes richer due to the option of gating: While negatively charged molecules remain stable, positive charging tends to destabilize the vertical molecular orientation even at our base temperature of 5 K. Attempts to charge a tip-attached molecule positively occasionally result in a collapse of the molecule onto the tip, whereas surface-standing PTCDA always collapses when positive charging is attempted.[11] These observations suggest that positive charging weakens the stabilization and sometimes completely eliminates the stabilizing local potential energy minimum. The molecule's variable behavior in response to positive charging moreover implies a dependency of the stabilization potential on the atomic configuration of the tip apex since this configuration is the only property that varies between individual experiments. We thus hypothesize that the stabilization potential of s-PTCDA on the Ag tip is typically larger than that on the adatom pedestal on Ag(111) (called "adatom surface" from now on) on which molecules always collapse upon positive charging. Finally, experiments attempting the creation of s-PTCDA on the bare Ag(111) surface turn out to be unsuccessful.

To explore this broad phenomenology computationally, we have to capture the corresponding variations in the Ag structure of both the tip and the surface. Especially the unknown tip geometry presents a formidable challenge which we address in the following section.

Tip–Molecule Bonding Geometries. Since there is only little experimental information about the SPM tip apex configuration, the actual bonding mode of PTCDA to the tip is unknown. On the most elementary level, this uncertainty boils down to the question of how many simultaneous Ag–O bonds are required to stabilize s-PTCDA on the tip. Two scenarios seem plausible: First, a metastable conformation featuring only a single chemical bond (Figure 1, right) as suggested by the lifting process in which the surface-adsorbed PTCDA is contacted with the SPM tip at *one* of its O_{carb} atoms and lifted off the surface. Second, a molecule attachment with two Ag–O bonds involving two neighboring O_{carb} atoms, similar to the known vertical conformation of the molecule on the adatom pedestal on Ag(111), which features *two* Ag–O_{carb} bonds.[11,17] (Figure 1, left).

To investigate the two scenarios in detail, we examine the bonding of PTCDA to a variety of different tip models (Figure 2). This allows us to determine, for example, how much the immediate surrounding of the tip–molecule binding site influences the bond properties. To study the one-bond scenario, we designed two pyramidal single-atom apex tip

models (*Tip 1* and *Tip 2*). For the two-bond scenario, we designed a set of eight tip models (*Tip 3–Tip 10*), all of which feature a flat Ag(111) area containing $5 \leq N \leq 40$ atoms (highlighted in Figure 2a) onto which two adatoms are placed as equivalent tip apexes. Since these models are effectively differently sized and shaped cutouts of an adatom–surface slab, their properties naturally converge to the adatom–surface case for very wide tips (e.g., *Tip 10* in Figure 2a).

Importantly, the two-atom apex tip models, *Tip 3–Tip 10*, are not necessarily "double tips" in the meaning of the term used in SPM, where it describes tips with two apex atoms at the same distance from the surface. Our tip models would only operate as double tips in SPM if their flat areas were exactly parallel to the imaged surface. This is not likely since, in experiment, there would be no preference for any specific crystal orientation of the tip apex region. Hence, our tip models are not in conflict with the experiments in which the use of double tips was avoided.

The bonding scenario also determines the degrees of freedom of the tip-attached molecule since rotation is possible around three axes in the one-bond scenario (Figure 2b), whereas there is only a single rotation axis in the two-bond scenario (Figure 2c). Mapping of the potential energy landscape thus requires two different approaches which are outlined below, starting with the more complicated one-bond scenario.

The configuration space of s-PTCDA attached to a single apex tip is primarily spanned by rotations of PTCDA around the apex atom, which we describe in a coordinate system that is fixed to the tip models and aligned with their high-symmetry directions (Figure 2b). The rotational and mirror symmetries of *Tip 1* and *Tip 2* allow limiting the conformation mapping to 1/6 of the half sphere below the apex. A rotation around the z-axis changes the molecule's azimuthal orientation, while rotations around the x or y axis bring it closer to the tip. To reduce the number of computed configurations, we map this "upward" rotation only in the high-symmetry x–z plane (dark pink in Figure 2b), effectively eliminating one rotational degree of freedom (around the x axis). The mapping thus proceeds by rotating PTCDA first around the z axis (angle α) and subsequently around the y axis (angle β) for three α values (0°, 90°, and 180°) and a series of β values with $\Delta\beta = 10°$. Small translations that optimize the geometry of the Ag–O_{carb} bond are accounted for by constrained structural relaxation (see Computational Methods). Since our constraining method allows also for small relaxations in β, the angle is remeasured after relaxation.

In the two-bond scenario, two adjacent O_{carb} atoms of PTCDA are bound to the two Ag apex atoms, which reduces the molecular degrees of freedom to a rotation around the respective O_{carb}–O_{carb} axis (tilt angle ξ) and small translations accounted for by constrained geometry relaxation (Figure 2c). Since our two-apex tip models are cutouts of a Ag(111) slab, we place the apexes as adatoms in the known D_1 or D_2 configurations.[11,17] In D_1, the atoms are located in two adjacent hollow sites of the same type (fcc or hcp sites, respectively), while D_2 features adatoms in nonidentical hollow sites (fcc–hcp combination). Previously, we found that the D_2 configuration provides slightly higher stability to s-PTCDA on the Ag(111) surface, specifically a 5 meV higher potential energy barrier against collapse.[17] Here, six of our tips feature a D_1 adatom configuration, while *Tip 7* and *Tip 9* feature a D_2 configuration.
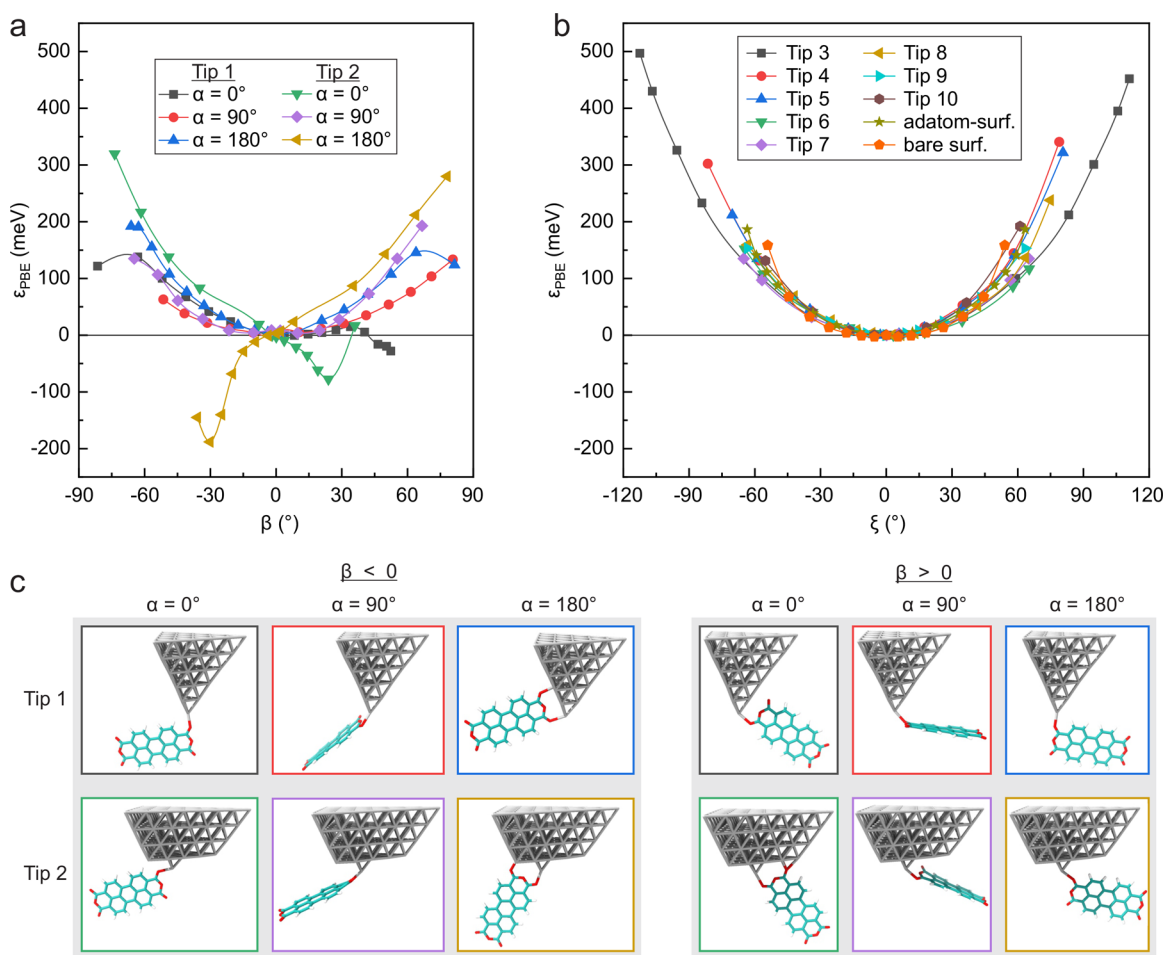
Figure 3. DFT-PBE potential surface of s-PTCDA. (a) PBE energies for the single-atom apex tip models (*Tip 1* and *Tip 2*) as a function of azimuthal molecule orientation α and tilt angle β. The geometries corresponding to the lowest and highest β value are displayed in panel (c). Spline fits of the data are a guide to the eye. (b) Potential energy profiles for s-PTCDA on all double-apex tip models, the bare and the adatom surface as a function of tilt angle ξ. For the corresponding geometries, see Figure 2a,c. (c) Geometries with minimal and maximal β values for the six curves in panel (a).

To put the results of our calculations for the various double-apex tip models into perspective, we also include the case of s-PTCDA on the adatom surface for which the structure is known and the hypothetical case of s-PTCDA standing on the *bare* Ag(111) surface (Figure 2c). Both configurations feature a single rotation axis similar to the two-apex tips. As motivated earlier, the first step of our analysis will now be a discussion of the (typically stabilizing) DFT-PBE potential energy surface, followed later by an analysis of the (destabilizing) long-range vdW potential.

Contributions of Covalent and Electrostatic Interactions to Molecular Stability. It was recently shown that the covalent and electrostatic interactions captured by DFT calculations with the PBE functional[32] stabilize s-PTCDA on the adatom surface against collapse.[17] In the following, we extend this picture by mapping the PBE potential energy landscape E_{PBE} of s-PTCDA attached to the variety of tip models described above. Our goal is to identify the most likely attachment scheme of PTCDA to the tip after loss of contact to the sample surface and to identify universal design principles that allow optimizing the stability of the vertical state. To obtain $E_{PBE} = E_{PBE}^{sys} - E_{PBE}^{tip} - E_{PBE}^{mol}$, we subtract the energy of the isolated systems of the tip (E_{PBE}^{tip}) and molecule (E_{PBE}^{mol}) from the energy of the combined system consisting

of the tip and molecule (E_{PBE}^{sys}). Although we do not yet discuss the long-range vdW energies E_{vdW} at this point, vdW interactions (calculated with the vdW^{surf} method) have, of course, been considered in the constrained geometry optimizations for all configurations presented below.

For each tip model, we plot the relative PBE energy $\epsilon_{PBE}(\alpha,\beta) = E_{PBE}(\alpha,\beta) - E_{PBE}(0°, 0°)$ or $\epsilon_{PBE}(\xi) = E_{PBE}(\xi) - E_{PBE}(0°)$, respectively, in Figure 3a and b. It shows that there is a clear qualitative difference between the one-bond and the two-bond scenarios. In the two-bond scenario in Figure 3b, the stabilizing potentials are quite similar across all tip and surface models, featuring a minimum at $\xi = 0°$ and torsional spring constants between $\kappa = 3 \times 10^{-20}$ Nm and $\kappa = 5 \times 10^{-20}$ Nm. This clearly demonstrates that the stabilizing potential must be primarily determined by the two Ag–O$_{carb}$ bonds and their immediate vicinity, which is the same for all two-apex tip models. The overall tip shape, on the other hand, seems to cause rather weak modifications of the potential, which could arise, for example, from electrostatic interactions between partial charges on PTCDA and Smoluchowski dipoles[41] of undercoordinated metal atoms at nearby edges and corners of the tip models.

Surprisingly, our results in Figure 3b also show that s-PTCDA experiences a stabilizing PBE potential even when
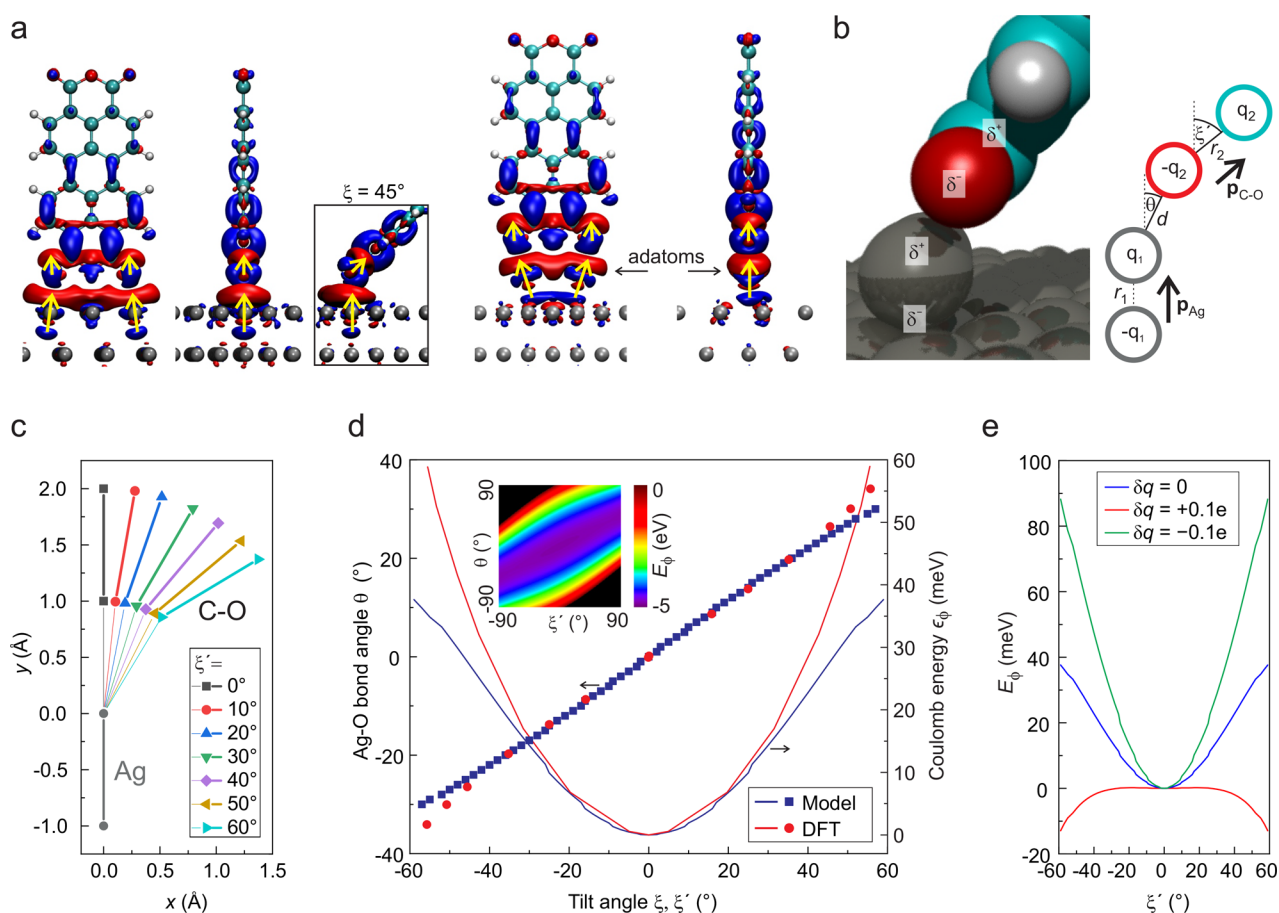
Figure 4. Electrostatic model of the stabilization mechanism. (a) Charge density difference $\Delta n(r) = n_{\text{system}}(r) - [n_{\text{molecule}}(r) + n_{\text{slab+adatoms}}(r)]$ for PTCDA on bare Ag(111) (left) and on the adatom surface (right). The isosurfaces are displayed for $-0.005\ \text{eÅ}^{-3} \leq \Delta n(r) \leq +0.005\ \text{eÅ}^{-3}$ and negative charge flows from red to blue regions. Local dipoles which are created or enhanced by the charge redistribution are indicated by yellow arrows. (b) Two-dipole model for the example of PTCDA on the adatom surface. Partial charges from Smoluchowski dipoles and bond dipoles are indicated in the space-filling model. Charges colored in gray represent the Ag adatom dipole; red charges represent the O atoms; and turquoise charges represent the nonaromatic C atoms. The angle ξ' equals the PTCDA tilt angle. (c) Lowest-energy configurations of the two dipoles for a series of tilt angles ξ'. (d) Properties of the two-dipole model for $r_1 = r_2 = d = 1$ Å and $q_1 = q_2 = 1e$. Red and blue symbols show the optimal (i.e., lowest energy) $\theta(\xi')$ relation for the dipole model (blue squares) and for the DFT calculation (red circles). The lines show the (relative) energy of the respective configurations (dipole model: blue, DFT: red). A scaling factor of 1/2 has been applied to the DFT data (see text). The inset shows the Coulomb energy $E_\phi(\theta, \xi')$ (eq 1) where regions with $E_\phi > 0$ are colored black. (e) Lowest-energy potentials $\epsilon_\phi(\xi')$ for a net charge δq which offsets each of the two charges that form the upper dipole $\mathbf{p}_{\text{C-O}}$. $\delta q = 0$ reproduces the blue curve from panel (d).

placed on the bare Ag(111) surface. This result suggests that no undercoordination of the metal atoms participating in the Ag$-$O$_{\text{carb}}$ bonds is required for stability. However, undercoordination still plays a central role in the actual manufacturing of s-PTCDA by SPM. The high strength of the O$_{\text{carb}}$$-$adatom bonds with a PBE energy of $E_{\text{PBE}} = -1.05$ eV allows breaking the bond between the tip and s-PTCDA by simple tip retraction (Figure 1 left), whereas the much weaker bonds between O$_{\text{carb}}$ and Ag atoms in the surface ($E_{\text{PBE}} = -0.29$ eV) break upon tip retraction, leaving the molecule on the tip (Figure 1, right). The configuration of a vertical PTCDA on bare Ag(111) and without contact to the tip would therefore be hardly accessible in an SPM manipulation experiment because it would have to involve breaking the tip$-$molecule bond, for example, by inelastic excitation of molecular vibrations via a tunneling current.

While all configurations in the two-bond scenario provide a similar level of stabilization, the situation is less clear in the one-bond scenario in Figure 3a. With only a single molecule$-$metal bond, there are many nonequivalent trajectories along

which the molecule can tilt toward the tip. First, our calculations reveal that the vertical molecule ($\beta = 0°$) can rotate around the z-axis practically without encountering a potential energy barrier since, at $\beta = 0°$, the energies for $\alpha = 0°$, $\alpha = 90°$, and $\alpha = 180°$ differ by less than 10 meV. Furthermore, it shows that the PBE potential $\epsilon_{\text{PBE}}(\alpha, \beta)$ does not generally stabilize the vertical molecular orientation, as it does in the two-bond scenario. Instead, the potential energy curves of *Tip 2* for $\alpha = 0°$ and $\alpha = 180°$ have minima around $\beta = +25°$ or $\beta = -30°$, respectively, and the $\beta = 0°$ minimum for *Tip 1* at the $\alpha = 0°$ orientation is negligibly shallow. Other tilt paths, on the other hand, do provide restoring forces with path-dependent torsional spring constants between $\kappa = 2.6 \times 10^{-20}$ Nm and $\kappa = 5 \times 10^{-20}$ Nm, similar to the two-bond scenario.

The variability of the potential energy profiles in the one-bond scenario is caused by the tendency of the adjacent (initially unbound) O$_{\text{carb}}$ atom to form a Ag$-$O bond as well. This transforms the one-bond scenario into a two-bond scenario as depicted in Figure 3c ($\alpha = 180°$ for $\beta < 0$ and $\alpha = 0°$ for $\beta > 0$). Since the energy scale of bond formation

substantially exceeds the energy scale of mere bond tilting, bond formation strongly deforms the potential energy surface and is typically always favored. The energy gain resulting from the second bond depends significantly on the Ag environment to which the second O_{carb} atom binds. This is exemplified by the E_{PBE} values for the bare and the adatom surface quoted above and by the different depths of the minima at $(0°, 25°)$ and $(180°, -30°)$ of *Tip 2*. As in the two-bond scenario, the remaining variations in the ϵ_{PBE} curves are likely related to inhomogeneous electrostatic potentials from Smoluchowski dipoles. For *Tip 1*, the second bond can only be established at rather large tilt angles β. At these geometries, our approach of constraining only a single C atom in the x direction and two C atoms in the y direction to fix both β and α while allowing a maximal freedom of structural relaxation (see Methods) fails insofar as the molecule adopts configurations where it does not bind to the apex atom anymore but favors binding to other atoms at the edge of the tip. In terms of a rigorous analysis, we have excluded the respective geometries, which does not affect any of our conclusions.

We obtain two central results from our calculations of the PBE energy E_{PBE} of s-PTCDA attached with one or two O_{carb} atoms to SPM tip models of various shapes. On one hand, we find that $Ag-O_{carb}$ bonds indeed stabilize the vertical orientation of s-PTCDA such that, in the hypothetical absence of all vdW interactions, the two-bond scenario would generally be stable. The single-bond scenario, on the other hand, is a very unlikely outcome of a PTCDA lifting experiment since there will usually be the option to form an energetically favorable second $Ag-O_{carb}$ bond. The possibility of the molecule to rotate freely around α at $\beta = 0°$ is important in this respect since it provides access to pathways along which this second bond can form without the necessity to overcome a potential energy barrier first. Hence, while the lifting of PTCDA always starts with a single $Ag-O_{carb}$ bond, our calculations suggest that a second bond to the tip will practically always form at some point of the lifting process, at the latest when the molecule is fully detached from the surface.

Point Charge Model of the Stabilization Mechanism. While the PBE energies clearly show the presence of a stabilizing potential, a deeper analysis is required to rationalize this finding and to formulate a simple design rule for increased stability. When s-PTCDA is placed on the adatom pedestal, the bonding causes a charge redistribution which can be visualized in a charge density difference plot (Figure 4a). Interestingly, this redistribution further increases dipoles which already exist in the isolated systems, namely, the polar C–O bonds of PTCDA and the Smoluchowski dipoles of the Ag adatoms (Figure 4a, right).[15] In the case of s-PTCDA on the bare Ag(111) surface, dipoles are created in the $Ag-O_{carb}$ bonding region as well (Figure 4a, left), despite the absence of dipoles in the isolated Ag(111) slab. Thus, both cases, with and without an adatom pedestal, are characterized by dipoles which point away from the surface. Importantly, the adatom Smoluchowski dipoles and even the $Ag-O_{carb}$ bond dipoles on the bare surface do not change their orientation when the molecule is tilted, while the C–O bond dipoles obviously do (Figure 4a).

Since we have already established that the stabilization must originate from the immediate surrounding of the $Ag-O_{carb}$ bonds, observing such local charge (re)distributions raises the question whether and how they are involved in the stabilization mechanism. To study this aspect, we set up a simple analytical

model in which the Ag-PTCDA bonding region is solely described by the interaction between four charges forming two dipoles (Figure 4b). The dipole which mimics the polar $Ag-O_{carb}$ bonds ($\mathbf{p}_{Ag}$) is fixed vertically to the surface, while the second one mimicking the polar C–O bonds ($\mathbf{p}_{C-O}$) has a variable orientation. More rigorously, the second dipole represents the projection of the C–O bond dipole onto the long molecular axis since all four point charges in our model are confined to one plane (Figure 4b).

The model is parametrized by seven quantities (r_1, r_2, d, θ, ξ', $q_1 > 0$, and $q_2 > 0$), and the electrostatic potential energy of this charge arrangement can be expressed as

$$
\begin{aligned}
E_\phi(\theta, \xi') = \frac{1}{4\pi\epsilon_0}[&-q_1q_2/d \\
&+q_1q_2/\sqrt{d^2 + r_2^2 - 2r_2d \times \cos(\pi + \theta - \xi')} \\
&+q_1q_2/\sqrt{d^2 + r_1^2 - 2r_1d \times \cos(\pi - \theta)} \\
&-q_1q_2/\sqrt{(d\sin(\theta) + r_2\sin(\xi'))^2 + (d\cos(\theta) + r_2\cos(\xi') + r_1)^2}]
\end{aligned}
$$

$$(1)$$

For our semiquantitative analysis, we use a parametrization with generic yet plausible values of $r_1 = r_2 = d = 1$ Å and $q_1 = q_2 = 1e$. The angles θ and ξ' have direct equivalents in the DFT calculations since θ corresponds to the angle between the $Ag-O_{carb}$ bond and a plane that is normal to the surface and passes through both Ag adatoms, while the tilt angle ξ' of the upper dipole $\mathbf{p}_{C-O}$ represents the molecule tilt angle ξ. The local lateral relaxation of the $Ag-O_{carb}$ bonds at a given ξ which we perform in DFT corresponds to choosing an angle θ which minimizes the Coulomb energy of the two-dipole system (Figure 4c). The respective function $E_\phi(\theta, \xi')$ (inset of Figure 4d) has minimal values along an almost linear $\theta(\xi')$ relation, which thus marks the minimal-energy path along which the O_{carb} atom moves in the two-dipole model upon tilting of the molecule ($\mathbf{p}_{C-O}$ dipole).

Two properties of the two-dipole model can be compared to our DFT results, namely, the outcome of the described relaxation expressed in the relation $\theta(\xi')$ and the ξ'-dependent relative Coulomb energy $\epsilon_\phi(\theta(\xi'), \xi') = E_\phi(\theta(\xi'), \xi') - E_\phi(0, 0)$ of the two-dipole system. The calculated $\theta(\xi')$ relation very well matches the corresponding relation of the full DFT calculation in the relevant range of $-60° < \xi < 60°$ (blue and red symbols in Figure 4d). Since, in the model, this relation does not depend on the values of q_1 and q_2 at all and is moreover rather insensitive to the choice of r_1, r_2, and d, the good correspondence to the DFT data is a robust conclusion. This indicates that the electrostatic forces as described by the two-dipole model could (at least partially) be the stabilization mechanism of s-PTCDA.

The plausibility of this assumption is further underpinned by a comparison of the tilt-angle-dependent relative Coulomb energy $\epsilon_\phi(\xi')$ (Figure 4d, blue curve) to the relative PBE-DFT total energy $\epsilon_{PBE}(\xi)$ (Figure 4d, red curve). Here, we have scaled $\epsilon_{PBE}(\xi)$ down to match the $\epsilon_\phi(\xi')$ curve in the range of $\pm 30°$ and found that a factor of $1/2$ was required. This is a reasonable result, given that there are two adatoms and $Ag-O_{carb}$ bonds and two C–O bonds in the s-PTCDA DFT calculation but only one dipole for each in the two-dipoles model. This rather good correspondence between $\epsilon_\phi(\xi')$ and $\epsilon_{PBE}(\xi)$ across a wide range of tilt angles also implies that our choice of model parameters r and q was reasonable and that
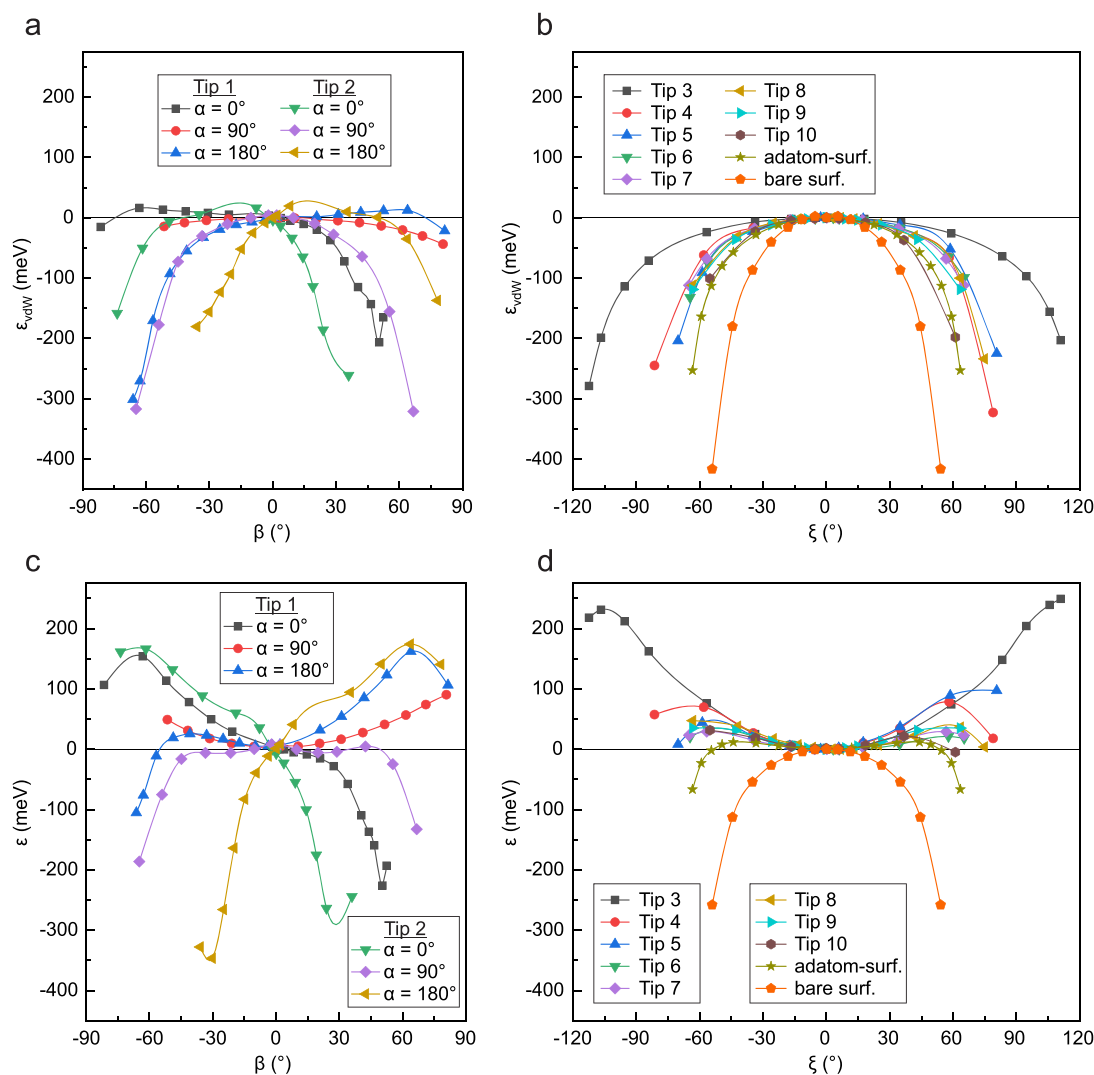
Figure 5. Relative vdW and total potentials in the one-bond and two-bond scenario. (a) vdW$^{\text{surf}}$ potentials $\epsilon_{\text{vdW}}(\beta)$ in the one-bond scenario. (b) vdW$^{\text{surf}}$ potentials $\epsilon_{\text{vdW}}(\xi)$ for the two-bond scenario. (c) Relative PBE + vdW$^{\text{surf}}$ total energy $\epsilon(\beta)$ for the one-bond scenario. (d) Relative PBE + vdW$^{\text{surf}}$ total energy $\epsilon(\xi)$ for the two-bond scenario. Spline fits of the data are a guide to the eye.

the two-dipole model can predict the correct order of magnitude of the stabilizing potential.

Finally, we turn to the experimental observation that a positive charging of s-PTCDA by appropriate gating destabilizes its vertical configuration,[11] particularly in the case of s-PTCDA on the adatom surface, where the stabilizing potential is rather shallow (Figure 5d). A negative charging of the molecule, on the other hand, does not cause any destabilization.[9,15,16] Using the two-dipole model, this observation can be attributed to an electrostatic effect as well. To mimic the charging, a small net charge δq is added simultaneously to both of the charges which form the dipole $\mathbf{p}_{\text{C–O}}$ that represents the molecule, such that they become $+q_2+\delta q$, and $-q_2+\delta q$. As a consequence, the $\epsilon_\phi(\xi')$ curve is flattened and finally inverted for $\delta q > 0$ (i.e., positive charging), while it becomes steeper for $\delta q < 0$ (negative charging) (Figure 4e), in correspondence to the experimental observations. This behavior emerges because tilting decreases the distance of the molecule charges $+q_2+\delta q$ and $-q_2+\delta q$ from $-q_1$. If δq is negative, this increases E_ϕ, while positive δq decreases E_ϕ.

Because the two-dipole model is based on point charges, it does not, for example, account for mutual (de)polarization

effects of the dipoles. Nevertheless, given its simplicity, the correspondence to the DFT calculations and experiments is convincing. In essence, the tilting of the upper one of two stacked and initially collinear dipoles provides the restoring force which stabilizes the vertical molecular orientation. With this explanation, we can derive a simple design rule aimed at engineering the stabilizing potential: Since at least a part of the stabilization emerges from similarly oriented dipoles in the molecule and the metal, the selective modification of these dipoles is the key to a modification of stability. We will show an example for such an engineering of electrostatics when demonstrating the application of our design rules in a later section.

Destabilizing van der Waals Interactions. Here, we turn to the long-range vdW interaction which provides the second contribution to the total potential energy of the molecule−metal structures and ultimately decides whether a configuration considered stable according to its PBE potential will indeed be stable. The vdW attraction between the molecule and the surface was found to cancel the stabilizing PBE potential for s-PTCDA on the adatom surface almost completely, allowing a thermally induced collapse already at T

= 10 K.[17] In the following, we discuss the general impact of vdW forces on the stability of standing molecules using our tip models and the bare and the adatom surface (Figure 5a,b). As in the case of covalent interactions, only relative vdW energies $\epsilon_{vdW} = E_{vdW} - E_{vdW}(0°)$ are relevant for the stability of s-PTCDA, where $E_{vdW}(0°)$ is the energy of the vertical configuration.

Depending on the context and aim, we either use the vdW^{surf} method[24,31] based on screened pairwise interactions or the MBD method,[28,29] which implicates a more accurate nonlocal description of vdW interactions at a higher computational cost. We use vdW^{surf} when exploring tip structures, an application in which vdW interactions are primarily determined by the atomic configuration of the tips and not by the difference between the two computational methods. We use MBD for our computational case studies (below) where the structures are precisely known and highly accurate vdW energies are beneficial.

Since the long-range metal–molecule vdW interaction is generally attractive, it does not provide any stabilization to s-PTCDA. In that sense, the data in Figures 5a and b can be interpreted rather straightforwardly in terms of changes in the distance between the tip or surface and PTCDA. In the two-bond scenario, the potential energy maximum is always at $\xi = 0°$ because any tilting of the molecule will bring *all* its atoms closer to the tip cluster or the surface (Figure 5b). The situation is different in the one-bond scenario, where tilting at ($\alpha = 0°$, $\beta < 0°$) and ($\alpha = 180°$, $\beta > 0°$) causes some C and O atoms in the vicinity of the Ag–O$_{carb}$ bond to initially withdraw from the tip, such that (shallow) potential energy maxima are found at nonzero β values instead (Figure 5a). Besides the general lack of stabilization, the variations among the individual $\epsilon_{vdW}(\beta)$ and $\epsilon_{vdW}(\xi)$ curves are quite pronounced. Since our computational method vdW^{surf} is, in essence, a pairwise approach, these variations can be interpreted straightforwardly by the Ag atom count in the tip models and by the tip sharpness. Sharper tips generally cause less vdW interactions as they have fewer atoms in the vicinity of the molecule. Consequently, s-PTCDA on the adatom surface and on the bare Ag(111) surface have the strongest vdW interactions since their Ag atom count is high and they are the analogue of completely blunt tips. Since this aspect is independent of the specific molecular species, it is valid for a broad range of SPM tip functionalizations.

Since we have studied a wide variety of tip models, we can estimate the region of influence around the molecule within which the tip structure has an impact on the stability of s-PTCDA. In Figure 6, we therefore compare the relative vdW energies for an exemplary tilt angle of $\xi = 35°$ for a range of tip "surface" areas (highlighted regions in Figure 2a) in the two-bond scenario. It shows that our biggest tip model (*Tip 10*) with 40 atoms in the "surface" plane already provides almost the same vdW energy gain upon tilting as the infinitely extended adatom surface. Hence, we can conclude that regions of the tip which are further from the apex atom than the length of the standing molecule itself have negligible influence on the stability.

A crucial result is found when comparing s-PTCDA on the adatom surface and on the bare Ag(111) surface (Figure 5b): In the absence of the adatom pedestal, the vdW interaction increases much more strongly when tilting the molecule, which is a consequence of the reduced molecule–surface distance. In combination with our results for the PBE potential, we can
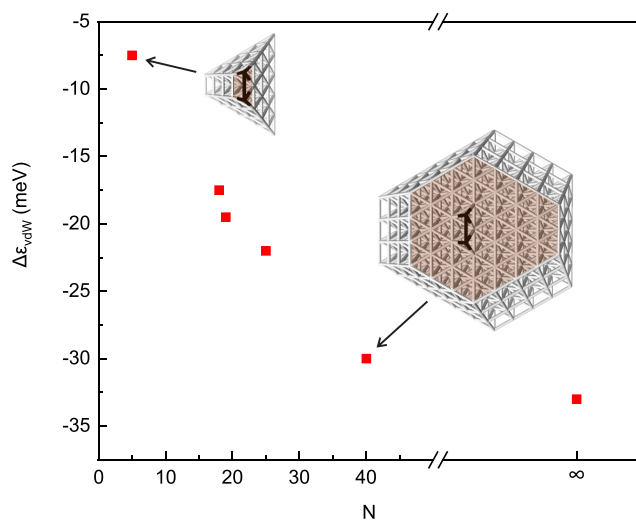

Figure 6. Relative vdW^{surf} energy $\epsilon_{vdW}(\xi = 35°)$ as a function of the number N of Ag atoms in the surface layer of the different tip models (highlighted area in Figure 2a). For the adatom surface, $N = \infty$.

thus conclude that the primary role of the adatom pedestal is not to enhance the stabilizing part of the potential but rather to act as a simple spacer separating PTCDA from the Ag atoms of the surface. This separation reduces the destabilizing effect of the vdW interaction considerably and allows s-PTCDA on the adatom surface to be stable. Besides its role as a spacer, the pedestal is, however, also essential for the practical fabrication of s-PTCDA on the adatom surface by SPM manipulation (see above).

As expected, the variations in ϵ_{vdW} also cause strong variations in the total relative energies $\epsilon = \epsilon_{PBE} + \epsilon_{vdW}$ among the different tip models (Figures 5c,d), such that the depth of the stabilizing potential varies by about 1 order of magnitude between *Tip 3* and the adatom surface. This is in general agreement with the experimental finding that s-PTCDA on the SPM tip is typically more stable and can often also survive positive charging.[9,15] Only on the bare Ag(111) surface do the destabilizing vdW interactions completely outweigh the stabilizing ϵ_{PBE} potential such that, even if it could be fabricated, s-PTCDA would not be stable on bare Ag(111) (Figure 5d). Moreover, the tilt paths along which the transition from a one-bond to a two-bond scenario occurs for *Tip 1* and *Tip 2* are clearly visible in the total relative energy plot (Figure 5c).

From our analysis of the long-range vdW interactions, we have obtained a second design rule for increased stability of metastable molecular structures on metals: The vdW attraction should be reduced as much as possible, which can happen either by increasing the distance between molecule and metal, as in the case of sharp tips or the adatom surface, or by reducing the number of atoms in the molecule. In the final part of our paper we will now close the loop and demonstrate that the deduced design principles indeed allow a systematic engineering of stability.

Computational Case Studies. Here we validate the two basic design principles that we have obtained in this study. Since our calculations for a variety of tip models have already provided ample examples for vdW engineering by modification of the metal structure, we will instead examine a reduction of the molecule size. The engineering of dipoles at the molecule–
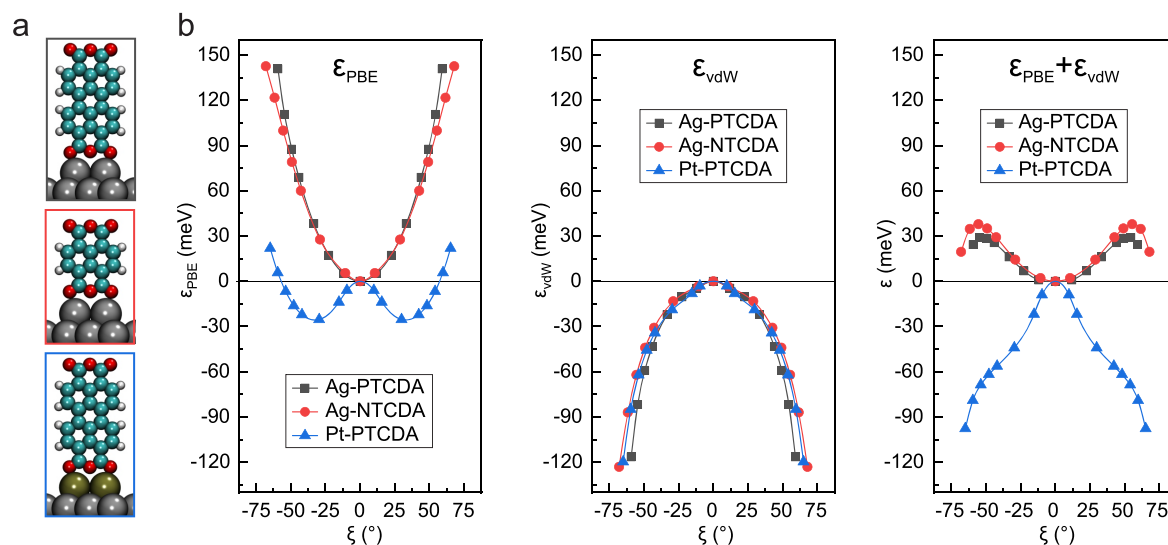
Figure 7. Engineering of the stabilization potential. (a) Structures of s-PTCDA on Ag (top) and Pt (bottom) adatoms and s-NTCDA on Ag adatoms (center) on D_2 adatom pedestals. (b) Relative energy profiles ϵ_{PBE} (left), ϵ_{vdW} using MBD (center) and $\epsilon = \epsilon_{PBE} + \epsilon_{vdW}$ (right) as a function of tilt angle ξ for the three examples in panel (a). The $\xi = 0°$ values for PTCDA on Pt are only estimated since the respective configuration is unstable under our minimal constraining.

metal bonding region will, on the other hand, be exemplified by changing the atomic species of the pedestal adatoms.

Consequently, we now examine the relative energy profiles $\epsilon(\xi) = \epsilon_{PBE}(\xi) + \epsilon_{vdW}(\xi)$ of two configurations which are both adaptations of s-PTCDA on the adatom surface (Figure 7a). On one hand, we decrease the vdW interaction by replacing PTCDA by the smaller NTCDA molecule which lacks one naphthalene unit but has the same functional groups. On the other hand, we engineer the dipoles in the bonding region by replacing the Ag adatom pedestal by a pedestal of Pt adatoms. Given the high Pt(111) work function of almost 6 eV,[42] Pt adatoms on Ag(111) are expected to create strong dipoles pointing toward the surface, while Ag adatoms on Ag(111) exhibit a rather strong dipole of 0.66 D pointing away from the surface.[15] According to our first design rule, this should destabilize PTCDA on a pedestal of Pt adatoms.

Relative PBE and vdW energies (using the MBD method) for a series of tilt angles ξ are shown in Figure 7b. Indeed, it shows that the stabilizing nature of the covalent Ag−O$_{carb}$ bond (ϵ_{PBE}) is barely altered when replacing PTCDA by the chemically similar NTCDA on the adatom surface. Using Pt adatoms beneath PTCDA, however, changes the picture completely. As expected from the two-dipole model, the oppositely oriented dipoles $\mathbf{p}_{Pt}$ and $\mathbf{p}_{C-O}$ now have a destabilizing effect on s-PTCDA, initially leading to a reduction in ϵ_{PBE} as the molecule is tilted. The DFT calculation, however, also reveals the limits of our simple point charge model which does not predict the observed increase in ϵ_{PBE} beyond $|\xi| = 30°$. This increase points toward a stabilization mechanism with two energy contributions: While we have turned the Coulomb interactions from stabilizing to destabilizing when switching from Ag to Pt adatoms, a second stability mechanism, possibly related to exchange interactions, is still in place. Irrespective of the precise mechanism, our design choice has practically removed the stabilizing effect of the $\epsilon_{PBE}(\xi)$ potential as intended, thus validating our first design principle. The presence of two stabilization mechanisms and the corresponding double-well potential (Figure 7b) could, on the other hand, even be an opportunity allowing the

fabrication of molecules in tilted configurations if the vdW interaction is sufficiently small.

The MBD vdW energies in Figure 7b validate also the second design principle, since replacing PTCDA by NTCDA yields the expected decrease in ϵ_{vdW}. The magnitude of this decrease of about 20−25% is, however, considerably below what would be expected from the heavy atom count alone (20 for NTCDA compared to 30 for PTCDA). This fact, again, illustrates the strong distance dependence of the vdW interactions: While NTCDA is smaller, its center of mass is also closer to the Ag(111) surface, partially compensating the size-related effect. The (unintended) reduction of ϵ_{vdW} for PTCDA on the Pt adatoms can be explained by the same effect. During tilting, PTCDA on Pt approaches the surface slower than PTCDA on Ag adatoms at the same tilt angles (this would correspond to a flatter $\theta(\xi)$ relation in Figure 4), which reduces the vdW interaction for PTCDA on Pt.

Ultimately, the stability of both scenarios, NTCDA on Ag and PTCDA on Pt adatoms, can only be judged based on the relative total energies $\epsilon = \epsilon_{PBE} + \epsilon_{vdW}$ plotted on the right of Figure 7b. It shows that the strategy derived from our design rules proved successful. NTCDA on the Ag adatom surface has a higher overall stabilization barrier than PTCDA on the same adatom type, while PTCDA on Pt adatoms has no stabilizing barrier at all. While this second case resembles PTCDA on bare Ag(111) (Figure 5d), the similarity is only superficial: In PTCDA on bare Ag(111), the destabilizing vdW interaction is increased, while for PTCDA on Pt adatoms the stabilization by electrostatic and covalent interactions is eliminated.

■ CONCLUSIONS

SPM-based fabrication is a powerful tool which grants access to unexplored molecular configurations with interesting properties and can draw from an almost infinite pool of molecular building blocks. Experimentally searching this vast chemical and configuration space for structures with a desired functionality can be extremely tedious if no clear strategy is available. Here, we have shown that computational nanostructure design can provide such strategies and straightforward

design rules. The results of our study are relevant for experiments and computation alike: The design rules for standing molecules can be directly employed to conceive future experiments, while our demonstration that computational nanostructure design is well suited to describe the potential energy profile of molecular nanostructures may trigger its application to new device ideas beyond standing molecules. Here, specifically the insight into the role played by dipole–dipole interactions in nanostructures is of very general nature. While we have applied our computational methods to the specific topic of metastable standing molecular configurations, it can probably be extended to other potential-energy-related aspects of molecular nanostructures and would also offer clear design rules. Studying the specific topic of metastability has the benefit that this aspect is tightly linked to functionality. This is exemplified by the role of s-PTCDA as a sensor, field emitter, and mechanical oscillator. Moreover, owing to their properties as well-defined, weakly coupled quantum systems, we also envision standing molecules to play a role in future quantum devices, for example, quantum sensors. The finding that PTCDA practically always attaches with two bonds to the SPM tip if retracted sufficiently from the surface not only has deepened our understanding of the role of s-PTCDA as a sensor in scanning quantum dot microscopy but also is important for SPM-based manipulation in general because the tip–molecule relation is that of the actuator and the work piece, and the presence of two bonds reduces the degrees of freedom of the latter. Summarizing, our findings mark an important step toward exploiting the full potentials of nanofabrication with scanning probe microscopes.

■ AUTHOR INFORMATION

Corresponding Author

  Christian Wagner − *Peter Grünberg Institute (PGI-3), Forschungszentrum Jülich, 52425 Jülich, Germany; Jülich Aachen Research Alliance (JARA), Fundamentals of Future Information Technology, Jülich, 52425 Jülich, Germany;* ○ orcid.org/0000-0002-2117-6289; Email: c.wagner@fz-juelich.de

Authors

  Hadi H. Arefi − *Peter Grünberg Institute (PGI-3), Forschungszentrum Jülich, 52425 Jülich, Germany; Jülich Aachen Research Alliance (JARA), Fundamentals of Future Information Technology, Jülich, 52425 Jülich, Germany; Helmholtz-Zentrum Berlin für Materialien und Energie, 14109 Berlin, Germany;* ○ orcid.org/0000-0003-4232-5076

  Daniel Corken − *Department of Chemistry, University of Warwick, CV4 7AL Coventry, U.K.*

  F. Stefan Tautz − *Peter Grünberg Institute (PGI-3), Forschungszentrum Jülich, 52425 Jülich, Germany; Jülich Aachen Research Alliance (JARA), Fundamentals of Future Information Technology, Jülich, 52425 Jülich, Germany; Experimentalphysik IV A, RWTH Aachen University, 52074 Aachen, Germany*

  Reinhard J. Maurer − *Department of Chemistry, University of Warwick, CV4 7AL Coventry, U.K.;* ○ orcid.org/0000-0002-3004-785X

Complete contact information is available at:
https://pubs.acs.org/10.1021/acs.jpcc.2c01514

Author Contributions

H.A., F.S.T., R.J.M., and C.W. conceived and designed this research. H.A. and D.C. performed and analyzed the DFT calculations. C.W. developed the dipole model. H.A., F.S.T., and C.W. wrote the paper with substantial contributions from R.J.M.

Notes

■ ACKNOWLEDGMENTS

■ REFERENCES

(1) Eigler, D. M.; Schweizer, E. K. Positioning single atoms with a scanning tunnelling microscope. *Nature* **1990**, *344*, 524−526.

(2) Heinrich, A. J.; Lutz, C. P.; Gupta, J. A.; Eigler, D. M. Molecule cascades. *Science* **2002**, *298*, 1381−1387.

(3) Nilius, N.; Wallis, T. M.; Ho, W. Development of one-dimensional band structure in artificial gold chains. *Science* **2002**, *297*, 1853−1856.

(4) Nazin, G. V.; Qiu, X. H.; Ho, W. Visualization and spectroscopy of a metal-molecule-metal bridge. *Science* **2003**, *302*, 77−81.

(5) Fölsch, S.; Martínez-Blanco, J.; Yang, J.; Kanisawa, K.; Erwin, S. C. Quantum dots with single-atom precision. *Nature Nanotechnol.* **2014**, *9*, 505−508.

(6) Kalff, F. E.; Rebergen, M. P.; Fahrenfort, E.; Girovsky, J.; Toskovic, R.; Lado, J. L.; Fernández-Rossier, J.; Otte, A. F. A kilobyte rewritable atomic memory. *Nature Nanotechnol.* **2016**, *11*, 926−929.

(7) Wagner, C.; Temirov, R.; Tautz, F. S. In *Molecular Architectonics The third stage of single molecule electronics*; Ogawa, T., Ed.; Springer Nature: Cham, Switzerland, 2017; pp 253−319.

(8) Green, M. F. B.; Esat, T.; Wagner, C.; Leinen, P.; Grötsch, A.; Tautz, F. S.; Temirov, R. Patterning a hydrogen-bonded molecular monolayer with a hand-controlled scanning probe microscope. *Beilstein Journal of Nanotechnology* **2014**, *5*, 1926−1932.

(9) Wagner, C.; Green, M. F. B.; Leinen, P.; Deilmann, T.; Krüger, P.; Rohlfing, M.; Temirov, R.; Tautz, F. S. Scanning quantum dot microscopy. *Phys. Rev. Lett.* **2015**, *115*, 026101.

(10) Natterer, F. D.; Yang, K.; Paul, W.; Willke, P.; Choi, T.; Greber, T.; Heinrich, A. J.; Lutz, C. P. J. Reading and writing single-atom magnets. *Nature* **2017**, *543*, 226−228.

(11) Esat, T.; Friedrich, N.; Tautz, F. S.; Temirov, R. A standing molecule as a single-electron field emitter. *Nature* **2018**, *558*, 573−576.

(12) Kocić, N.; Blank, D.; Abufager, P.; Lorente, N.; Decurtins, S.; Liu, S. X.; Repp, J. Implementing functionality in molecular self-sssembled monolayers. *Nano Lett.* **2019**, *19*, 2750−2757.

(13) Huff, T. R.; Dienel, T.; Rashidi, M.; Achal, R.; Livadaru, L.; Croshaw, J.; Wolkow, R. A. Electrostatic landscape of a hydrogen-terminated silicon surface probed by a moveable quantum dot. *ACS Nano* **2019**, *13*, 10566−10575.

(14) Leinen, P.; Esders, M.; Schütt, K. T.; Wagner, C.; Müller, K.-R.; Tautz, F. S. Autonomous robotic nanofabrication with reinforcement learning. *Science Advances* **2020**, *6*, No. eabb6987.

(15) Wagner, C.; Green, M. F.; Maiworm, M.; Leinen, P.; Esat, T.; Ferri, N.; Friedrich, N.; Findeisen, R.; Tkatchenko, A.; Temirov, R.; Tautz, F. S. Quantitative imaging of electric surface potentials with single-atom sensitivity. *Nat. Mater.* **2019**, *18*, 853−859.

(16) Temirov, R.; Green, M. F. B.; Friedrich, N.; Leinen, P.; Esat, T.; Chmielniak, P.; Sarwar, S.; Rawson, J.; Kögerler, P.; Wagner, C.; Rohlfing, M.; Tautz, F. S. Molecular model of a quantum dot beyond the constant interaction approximation. *Phys. Rev. Lett.* **2018**, *120*, 206801.

(17) Knol, M.; Arefi, H. H.; Corken, D.; Gardner, J.; Tautz, F. S.; Maurer, R. J.; Wagner, C. The stabilization potential of a standing molecule. *Science Advances* **2021**, *7*, No. eabj9751.

(18) Rohlfing, M.; Bredow, T. Binding energy of adsorbates on a noble-metal surface: exchange and correlation effects. *Phys. Rev. Lett.* **2008**, *101*, 266106.

(19) Romaner, L.; Nabok, D.; Puschnig, P.; Zojer, E.; Ambrosch-Draxl, C. Theoretical study of PTCDA adsorbed on the coinage metal surfaces, Ag(111), Au(111) and Cu(111). *New J. Phys.* **2009**, *11*, 053010.

(20) Rusu, P. C.; Giovannetti, G.; Weijtens, C.; Coehoorn, R.; Brocks, G. Work function pinning at metal-organic interfaces. *J. Phys. Chem. C* **2009**, *113*, 9974−9977.

(21) Tkatchenko, A.; Romaner, L.; Hofmann, O. T.; Zojer, E.; Ambrosch-Draxl, C.; Scheffler, M. Van der Waals interactions between organic adsorbates and at organic/inorganic interfaces. *MRS Bull.* **2010**, *35*, 435−442.

(22) Rusu, P. C.; Giovannetti, G.; Weijtens, C.; Coehoorn, R.; Brocks, G. First-principles study of the dipole layer formation at metal-organic interfaces. *Phys. Rev. B* **2010**, *81*, 125403.

(23) Maurer, R. J.; Ruiz, V. G.; Tkatchenko, A. Many-body dispersion effects in the binding of adsorbates on metal surfaces. *J. Chem. Phys.* **2015**, *143*, 102808.

(24) Ruiz, V. G.; Liu, W.; Tkatchenko, A. Density-functional theory with screened van der Waals interactions applied to atomic and molecular adsorbates on close-packed and non-close-packed surfaces. *Phys. Rev. B* **2016**, *93*, 035118.

(25) Arefi, H. H.; Fagas, G. Chemical trends in the work function of modified Si(111) surfaces: A DFT study. *J. Phys. Chem. C* **2014**, *118*, 14346−14354.

(26) Arefi, H. H.; Nolan, M.; Fagas, G. Density functional theory with van der waals corrections study of the adsorption of alkyl, alkylthiol, alkoxyl, and amino-alkyl chains on the H:Si(111) surface. *Langmuir* **2014**, *30*, 13255−13265.

(27) Tkatchenko, A.; Scheffler, M. Accurate molecular van der Waals interactions from ground-state electron density and free-atom reference data. *Phys. Rev. Lett.* **2009**, *102*, 073005.

(28) Tkatchenko, A.; DiStasio, R. a.; Car, R.; Scheffler, M. Accurate and efficient method for many-body van der Waals interactions. *Phys. Rev. Lett.* **2012**, *108*, 236402.

(29) DiStasio, R. A., Jr.; von Lilienfeld, O. A.; Tkatchenko, A. Collective many-body van der Waals interactions in molecular systems. *Proc. Natl. Acad. Sci. U.S.A.* **2012**, *109*, 14791−14795.

(30) Ambrosetti, A.; Reilly, A. M.; DiStasio, R. A., Jr.; Tkatchenko, A. Long-range correlation energy calculated from coupled atomic response functions response functions. *J. Chem. Phys.* **2014**, *140*, 18A508.

(31) Ruiz, V. G.; Liu, W.; Zojer, E.; Scheffler, M.; Tkatchenko, A. Density-functional theory with screened van der Waals interactions for the modeling of hybrid inorganic-organic systems. *Phys. Rev. Lett.* **2012**, *108*, 146103.

(32) Perdew, J. P.; Burke, K.; Ernzerhof, M. Generalized gradient approximation made simple. *Phys. Rev. Lett.* **1996**, *77*, 3865−3868.

(33) Blum, V.; Gehrke, R.; Hanke, F.; Havu, P.; Havu, V.; Ren, X.; Reuter, K.; Scheffler, M. Ab initio molecular simulations with numeric atom-centered orbitals. *Comput. Phys. Commun.* **2009**, *180*, 2175−2196.

(34) Van Lenthe, E.; Baerends, E. J.; Snijders, J. G. Relativistic total energy using regular approximations. *J. Chem. Phys.* **1994**, *101*, 9783−9792.

(35) Monkhorst, H. J.; Pack, J. D. Special points for Brillouin-zone integrations. *Phys. Rev. B* **1976**, *13*, 5188−5192.

(36) Fu, C. L.; Ho, K. M. First-principles calculation of the equilibrium ground-state properties of transition metals: Applications to Nb and Mo. *Phys. Rev. B* **1983**, *28*, 5480−5486.

(37) Zhang, I. Y.; Ren, X.; Rinke, P.; Blum, V.; Scheffler, M. Numeric atom-centered-orbital basis sets with valence-correlation consistency from H to Ar. *New J. Phys.* **2013**, *15*, 123033.

(38) Fournier, N.; Wagner, C.; Weiss, C.; Temirov, R.; Tautz, F. S. Force-controlled lifting of molecular wires. *Phys. Rev. B* **2011**, *84*, 035435.

(39) Wagner, C.; Fournier, N.; Tautz, F. S.; Temirov, R. Measurement of the binding energies of the organic-metal perylene-teracarboxylic-dianhydride/Au(111) bonds by molecular manipulation using an atomic force microscope. *Phys. Rev. Lett.* **2012**, *109*, 076102.

(40) Wagner, C.; Fournier, N.; Ruiz, V. G.; Li, C.; Müllen, K.; Rohlfing, M.; Tkatchenko, A.; Temirov, R.; Tautz, F. S. Non-additivity of molecule-surface van der Waals potentials from force measurements. *Nat. Commun.* **2014**, *5*, 5568.

(41) Smoluchowski, R. Anisotropy of the electronic work function of metals. *Phys. Rev.* **1941**, *60*, 661−674.

(42) Derry, G. N.; Kern, M. E.; Worth, E. H. Recommended values of clean metal surface work functions. *Journal of Vacuum Science & Technology A* **2015**, *33*, 060801.